Performance evaluation of a waste-heat driven adsorption system for automotive air-conditioning: Part I - Modeling and experimental validation

M. Verde **(UPV)**
K. Harby **(UPV)**
R. de Boer **(ECN)**
J. M. Corber **(UPV)**

July 2016
ECN-W--16-027

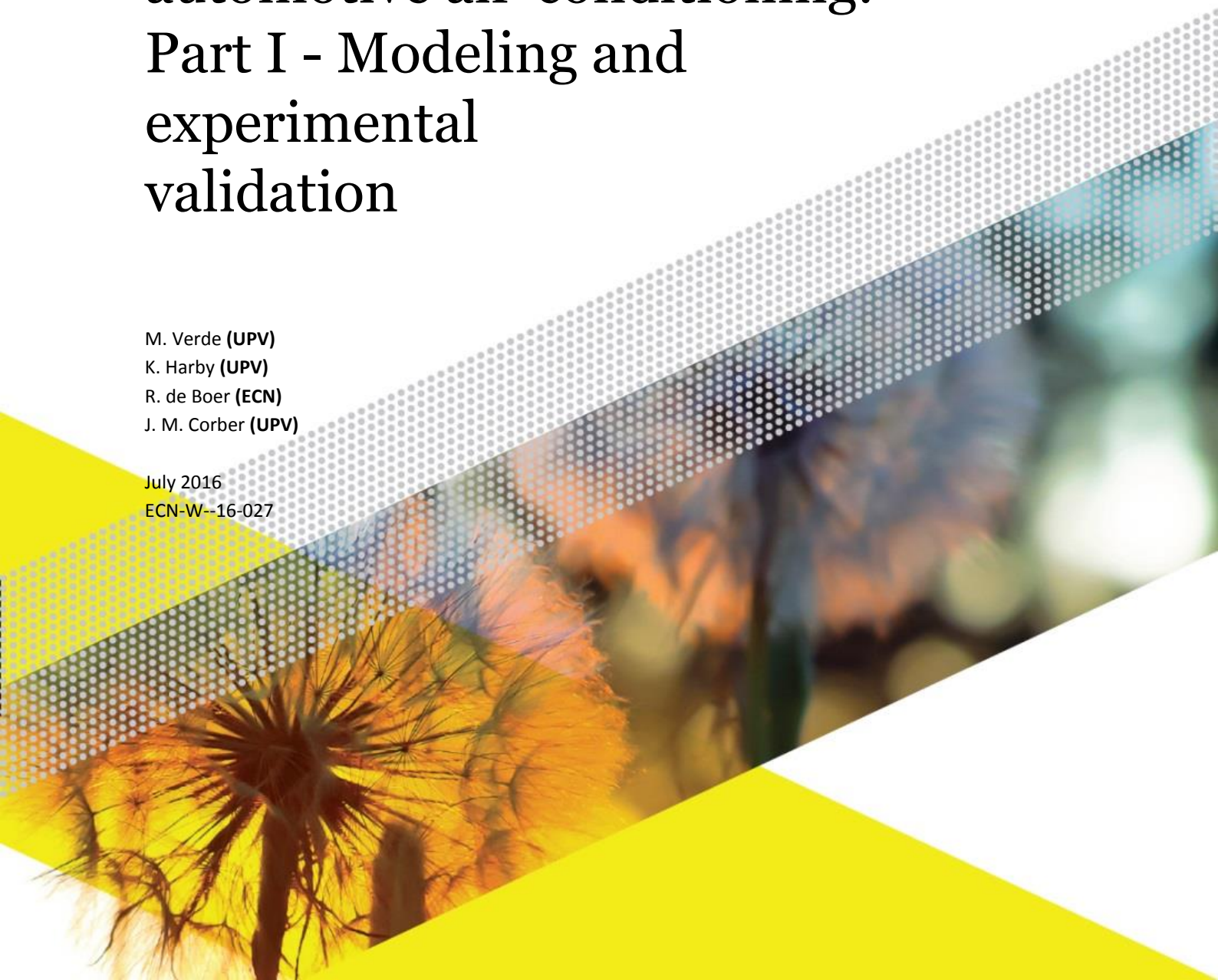

Energy 116 (2016) 526–538

Contents lists available at ScienceDirect

Energy

journal homepage: www.elsevier.com/locate/energy

Performance evaluation of a waste-heat driven adsorption system for automotive air-conditioning: Part I – Modeling and experimental validation

M. Verde [a], K. Harby [a, b, *], Robert de Boer [c], José M. Corberán [a]

[a] Instituto de Ingeniería Energética, Universidad Politécnica de Valencia, Camino de Vera 14, ES 46022 Valencia, Spain
[b] Mechanical Power Engineering and Energy Department, Faculty of Engineering, Minia University, 61519, Minia, Egypt
[c] Energy Research Centre of the Netherlands, ECN, PO Box 1, 1755 ZG, Petten, The Netherlands

ARTICLE INFO

Article history:
Received 12 July 2016
Received in revised form
27 August 2016
Accepted 23 September 2016

Keywords:
Automotive A/C system
Adsorption chiller
Waste heat recovery
Experiments
Modeling and simulation

ABSTRACT

Adsorption systems driven by engine waste heat are one of the possible alternatives to the conventional automobile air conditioning in terms of energy savings and environmental issues. Assessment of this issue are carried in a two-part study. In this first part I, theoretical and experimental investigations were performed on a two bed, silica gel adsorption chiller for automotive applications. A prototype adsorption system with a total weight of about 86 kg was developed and tested to driven by low-grade waste heat. The single adsorbent bed consisted of three plate-fin heat exchangers connected in parallel. An improved non-equilibrium lumped parameter model was developed to predict the transient performance of the system. The model is fully dynamic and takes into account the mass transfer resistance and pressure drop for each component of the system. The results showed that the model is able to accurately predict the dynamic performance of the system under different operating conditions and configuration modes with a short calculation time. The tested chiller was able to produce an average cooling capacity of about 2.1 kW with a COP of 0.35 at the rated operating conditions. Heat recovery system results in increasing the COP by 43% and the cooling power by 4%.

1. Introduction

Energy savings and environment-friendly applications are becoming one of the important topics nowadays due to the rapid population growth and increase in the standard of living. Hazardous gasses from automobiles exhausts and chemically synthetic refrigerants used in the traditional vapor-compression refrigeration cycles (VCRC) are of the major pollutants of our environment [1,2]. In addition, transportation is one of the major users of primary energy and burns most of the world petroleum. The most common method for refrigeration and air conditioning systems in different applications is employing VCRC due to its high COP [3,4]. However, the use of these systems leads to a considerable high-grade energy consumption and environmental pollution. The negative impacts of the VCRS become more pronounced in automotive and transportation applications where the compressor is powered by mechanical energy from the internal combustion engine.

Thermally driven adsorption cooling systems (ACSs) can use natural working fluids (such as water or ammonia) as a refrigerant and have the ability to be driven by a low-grade heat source such as solar energy and waste heat from automobile engines or industrial applications [5,6]. Therefore, these systems can be considered one of the possible alternatives to VCRSs (e.g. automobile applications) in terms of energy savings and environmental issues. The exhaust heat from the engine can be used to supply the required thermal energy input to the adsorption chiller. The waste heat usually constitutes 60–70% of the total energy used in internal combustion engines (ICE) during energy conversion processes [7,8].

Different experimental and theoretical studies have been performed on the adsorption cooling systems processes [9–13]. The majority of the existing studies are related to the development of mathematical models. Recent developments are focusing on dynamic models which can give a more clear idea about the transient behavior of the heat and mass transfer processes in the adsorbent bed, especially when heat-source is variable, as in the case of

* Corresponding author. Instituto de Ingeniería Energética, Universidad Politécnica de Valencia, Camino de Vera 14, ES 46022 Valencia, Spain.
E-mail address: khaledharby8@yahoo.com (K. Harby).

http://dx.doi.org/10.1016/j.energy.2016.09.113
0360-5442/

automobile applications. The majority of researchers propose zero-dimensional models [14–23] while some have focused on one-dimensional models [24–27]. Two and three-dimensional models can also be found in the literature by Refs. [28–32] and [33,34] respectively. However, the main differences between the different models generally occur in the simplifying assumptions, numerical solution method, components design and application of the modeled system. Table 1 listed a summary survey of experimental and theoretical studies based on adsorption cooling systems driven by engine waste heat.

It can be noticed that systems which have lower heat source temperature have higher COP than those with higher heat source temperature. It may be due to the fact that the heat losses related to the alternate heating/cooling of the bed increase by raising the bed's temperature. Silica gel-water pair can be efficiently used with a maximum desorption temperature of 80–90 °C, which is suitable for adsorption systems driven by low-temperature heat sources, as it is the case of the engine cooling circuit of automobiles which normally lies between 90 and 95 °C. Few experimental data and calculations on adsorption chillers powered by engine waste heat with heat recovery system can be found in the literature [44]. The system performance with heat recovery could be improved up to 50% [45–47].

All the existing models up so far contain certain simplifications in the basic equations that result sometimes in numerical instabilities Douss et al. [48]. Therefore, there is a need for more reliable dynamic models and, in particular, to predict the entire system components of any sorption systems includes the evaporator, condenser, adsorbent beds, valves, and other heat exchangers.

In part I of this study, modeling and experimental testing of an adsorption chiller system powered by engine waste heat is investigated. The system performance was evaluated with and without heat recovery operation mode. An improved non-equilibrium dynamic model of the adsorption/desorption process in transient regime is developed to simulate the behavior of the silica gel (Sorbil A)/water adsorption system under different configuration modes. The model incorporates all system components in order to simulate the full dynamic behavior of the entire system. In addition, the model can estimate the instantaneous operation, performance, and efficiency of each component. Moreover, the kinetics of the desorption/adsorption processes, the thermal inertia of all the involved components, including the fluid circuits, and the operation of the valves between components can be estimated. This will allow understanding the non-equilibrium adsorption/desorption process in transient regime.

As a comparison between the proposed model and those existent in the literature is that the flow between the components is based on the pressure difference between them. The pressure inside the adsorber is based on state equation and mass conversation. This makes the model able to capture the most important characteristics of the dynamics of the system. In addition, different valve operation strategies or automatic operation (reed valves) can be evaluated with the present model. However, the developed model has been validated with the actual experimental measurements in dynamic conditions and under different operation strategies such as the inclusion of a heat recovery process. The experimental data were performed at the Energy research Centre of the Netherlands, Petten (ECN).

In part II of this study, the validated model is used to simulate and optimize the transient performance of an on-board adsorption chiller (implemented in a vehicle) under actual operating conditions and obtain comfortable temperatures in the cabin[4].

2. Design and description of the adsorption system

The cooling water temperature at the outlet of automotive engines normally lies between 90 and 95 °C [5]. Therefore, a great amount of thermal energy (waste heat) can be recovered from the engine's coolant cycle at those temperatures. In addition, the water temperature could be increased by heat recovery operation from the exhaust gasses in order to provide an increased temperature heat source.

The proposed adsorption system was designed and tested under the framework of the TOPMACS project for automotive air conditioning applications [49] where the experimental tests are performed at the ECN laboratories. The system consists of two sorption beds named BED 1 and BED 2 connected to a condenser and an evaporator, an expansion device and four check valves to direct the refrigerant vapor flow, a condensate valve connected to a liquid level control in the evaporator and four three way valves to direct the heating and cooling water circuits alternately to both adsorbent beds as shown in Fig. 1. As shown in the figure, the system also involves three independent secondary water loops: a secondary water loop to heat the bed (Heating Water Loop), a secondary water loop to cool first the condenser and then the bed (Cooling Water Loop), and a secondary water loop to provide heat to the refrigerant in the evaporator (Chilled Water Loop). The adsorbent beds operate in counter-phase in order to allow a continuous useful effect: when the first bed is in cooling mode the second one is in regeneration mode. The hot water is sent to one of the two beds, depending on the position of the valves in the liquid circuit. The cooling water is

Table 1
Summary of studies related to the use of engine waste heat (exhaust gasses and/or water coolant) to drive adsorption cooling systems.

Heat source	Ref.	Heat source (°C)	Pair	SCP Wkg-1	COP	Cooling temp (°C)	Cooling power (KW)	Application	Study type
Engine waste heat gasses	[35]	210–230	zeolite–water	N/A	0.38	18	3.4	locomotive	E
	[8]	350–450	zeolite–water	164–200	0.25	10	6.5–10.0	locomotive	E[a] + T[a]
	[36]	400	zeolite–water	N/A	0.2–0.3	7	5	locomotive	E
	[14]	255–296	zeolite–water	25.7	0.38	10	45	truck	E + T
	[37]	200–250	zeolite–water	N/A	0.25	3.0–5.0	2.8–4.0	locomotive	E
	[38]	325	zeolite 13x –water	180	0.4	0.7–16.2	0.002–0.0105	truck	E
	[39]	220–250	zeolite–water	N/A	0.21	5–18	3.0–4.2	locomotive	E
	[16]	200	activated carbon–methanol	400	0.25	15–25	0.65	Diesel engine	T
	[17]	250	zeolite–water	N/A	0.436	7–15	2.015	truck	E + T
	[18]	80–90	zeolite–water	N/A	0.6	10	5	truck	E + T
	[40]	400–600	zeolite–water	N/A	N/A	11	2.5	truck	E
Engine coolant water	[19]	270–450	zeolite 13x –water	45	0.41	10	N/A	automobile	T
	[41]	90	activated carbon–ammonia	650–800	0.22	20	1.6–2.0	automobile	E
	[42]	87	silica gel–water	208	0.62	12	3.6	automobile	E
	[43]	90	N/A	300–600	0.25–0.45	8–14	1–2.3	truck	E

[a] E–refers to experimental study and T refers to theoretical study.

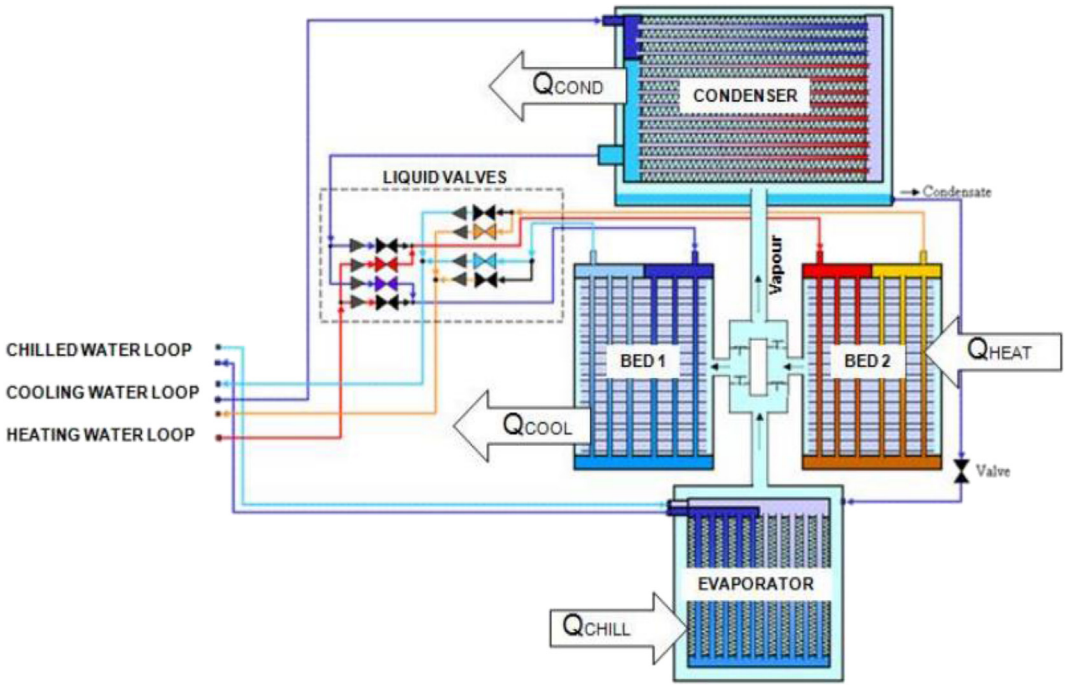

Fig. 1. Schematic diagram of the considered adsorption cooling system, detailed view.

first sent to the condenser and then through the valves to the other bed. The chilled water circuit is directly fed to the evaporator.

Fig. 2(a) shows a photo of the thermal compressor (Two beds) of the adsorption system consists of two beds. Each bed has three tube-fin heat exchangers connected in parallel as shown in the picture of Fig. 2 (b). Physically, the flat tube-fin heat exchanger is constructed of flat channel tubes covered with uniformly spaced flat fins to increase the heat transfer to the adsorbent. This kind of heat exchangers (HE) is available at low cost in the market as it is used as an evaporator for conventional automotive air conditioning systems. In addition, these type of HE is made from aluminum, having the advantages of both low weight and low thermal capacity compared with other types of heat exchangers. The weight of each adsorbent bed heat exchanger (except the headers) is approximately 1.012 kg.

The fin side of each heat exchanger is filled with approximate 1 kg of silica gel (Sorbil A) grains. The beds are connected to a housing that contains check valves (reed type). The condenser has three automotive evaporator heat exchangers connected in parallel and included in a stainless steel casing. On the other hand, the evaporator consists of four tube-fin heat exchangers (automotive heater cores types). Finally, the overall weight of the prototype system is 86 kg, not including the weight of the water in the circuits for heating, cooling and chilling, the refrigerant water in the evaporator, and the thermal insulation.

All secondary water circuits (heating, cooling and chilled water circuit) contained a temperature controlled water storage and a pump. To determine the thermal powers, each circuit was equipped with a flow sensor (Burkert), temperature sensors (PT100) of which the deviations are $0.3 + 0.005t$ °C (t is the tested temperature value) at the inlet and outlet, and a wet pressure difference sensor to measure the pressure drop. Furthermore, temperature sensors are installed inside the beds, the evaporator and the condenser and pressure sensors are mounted on the condenser and evaporator and on both beds. All sensors for the measurements were checked before and corrected for deviations. Components installed (adsorbent beds, temperature and pressure gauges, flow meters, valves, and pumps) are electronically managed. A data acquisition and control system was realized by a specific software written in the LabVIEW language. A PLC system is installed to control the electrical equipment such as pumps and liquid valves, and to acquire readings from the temperature, pressure and flow sensors. The

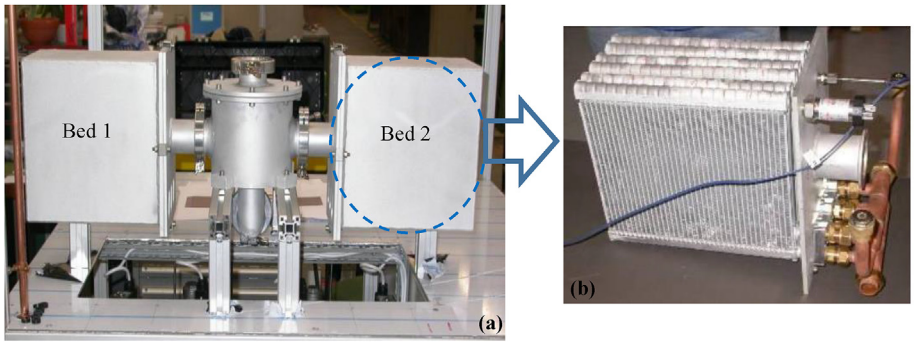

Fig. 2. **(a)** Two sorption beds connected to the central housing that contains the refrigerant check valves. **(b)** One sorption bed assembly.

repeated heating and cooling of the beds is controlled by four electromagnetic three-way liquid valves.

In order to assess the performance of the system, the experimental tests have been performed at two different operations (configurations) modes of the liquid valves of the heating and cooling water circuit as shown in Fig. 3. i) The first operation mode had no time delay between the switching of the outlet and inlet valves. ii) The second operation mode included a delay time between the switching of the liquid circuit valves in order to decrease the heat losses due to the alternate use of the hot and cooling water flows (heat recovery). The test-rig allows the fully automatic operation of the system and the management of different control strategies.

If the temperature difference between the inlet and outlet is smaller than a predefined value (e.g. 1 K), the inlet valves (V-1and V-3) will switch. The outlet valves (V-2 and V-4) will switch with a time delay with respect to the inlet valves. The time delay is set to such a value that at the moment of switching the outlet temperatures are almost identical and within the range of the average temperatures of the heating and cooling water circuit. The time delay prevents hot water remaining inside the bed to be sent directly to the cooling circuit and cooling water remaining in the cold bed to be sent to the heating circuit. The result is that some heat of the water stored in the bed is always returned to the hot water circuit, and the cold water stored in the other bed is sent to the cooling water circuit. In this operation mode a part of the sensible heat contained in the liquid circuits is recovered, with the aim to increase the COP.

3. Mathematical modeling

3.1. Assumptions

- Uniform temperature distribution in each component at any instant.
- Non-equilibrium conditions at the adsorption/desorption beds.
- The empty space in the adsorbent heat exchanger is filled in with water vapor. Consequently, the pressure at the beds depends on the instantaneous mass of vapor contained inside and its temperature.
- Perfect gas behavior has been assumed.
- The flow of water between the adsorbent beds, the condenser, and the evaporator are dominated by the pressure difference between these devices and the status of the valves.
- Liquid water is assumed in thermodynamic equilibrium corresponding to saturation conditions.

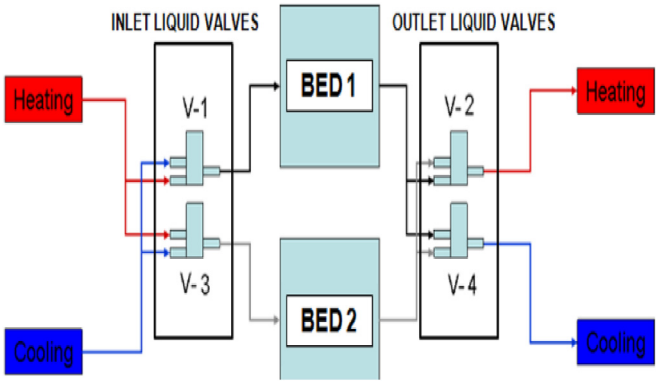

Fig. 3. Layout of the liquid valves of heating and cooling circuits for the two beds system.

3.2. Adsorption isotherm and kinetics

The adsorbent material employed was a silica gel (Sorbsil A) manufactured by Ineos Group Limited [50]. The thermo-physical properties of the selected silica gel (Sorbsil A) is shown in Table 2.

The equilibrium water uptake of silica gel (Sorbil A)/water pair is correlated by the following equation [51]:

$$\ln P_b = A(w_{eq}) + \frac{B(w_{eq})}{T_b} \tag{1}$$

where, the parameters A and B are characteristics of the adsorbent/adsorbate interaction and describe a set of isosteres:

$$A(w_{eq}) = a_0 + a_1(w_{eq}) + a_2(w_{eq})^2 + a_3(w_{eq})^3 \tag{2}$$

$$B(w_{eq}) = b_0 + b_1(w_{eq}) + b_2(w_{eq})^2 + b_3(w_{eq})^3 \tag{3}$$

The numerical values of the constants a and b ($i = 0, 1, 2, 3$) were obtained experimentally for the silica gel/water pair by Restuccia et al. [52].

In practical, the non-equilibrium conditions of the adsorbent material occur in adsorption systems, so the adsorption rate depends on the difference between the instantaneous uptake at the bed and the one that would be obtained at the equilibrium conditions (w_{eq}) Sakoda et al. [53]:

$$\frac{dw_b}{dt} = k_m(w_{eq} - w_b) \tag{4}$$

where, k_m is the overall mass transfer coefficient for Sorbil A/water pair which can be given by:

$$k_m = \frac{15D_s}{R_p^2} \tag{5}$$

where, R_p is the silica gel radios and D_s is the surface diffusivity which is defined by Arrhenius equation as,

$$D_s = D_{s0}\exp\left(-\frac{E_a}{RT_b}\right) \tag{6}$$

Combining Eqs. (5) and (6) in Eq. (4):

$$\frac{dw_b}{dt} = k_1 e^{-k_2/T_b}(w_{eq} - w_b) \tag{7}$$

where, $k_1 = 15D_{so}/R_p^2$ and $k_2 = E_a/R$ have constant values which have been taken from Sakoda et al. [53].

Isosteric heat of adsorption (Δh_{ad}) is not considered constant in the present study, as often occurs in the literature, but depends on the amount of adsorbed water. The isosteric heat of adsorption is extracted experimentally for Sorbil A/water pair [52]:

Table 2
The thermo-physical properties of silica gel (Sorbsil A).

Parameter	Value
Grain size, mm	0.2–1.0
w, kg kg^{-1}	0.1781
Δh_{ad}, kj kg^{-1}	3115.9
C_P, Jkg^{-1} K^{-1}	750
Surface area, m^2 g^{-1}	800
D_{s0},m^2 s^{-1}	2.54×10^{-4}
E_a, kJ mol^{-1}	42

$$\Delta h_{ad}(w_b) = -\left(b_0 + b_1 w_b + b_2 w_b^2 + b_3 w_b^3\right)\frac{R}{M_w} \quad (8)$$

The numerical values of the coefficients b (i = 0, 1, 2, 3) are also given for the present pair [52].

3.3. Mass and energy balance equations

The governing equations are derived from the energy and mass balance and by the corresponding thermodynamic relationships for the different components of the system.

3.3.1. Adsorber and desorber model

Fig. 4 shows a control volume (red dashed line) for which the energy balance applies on a single adsorbent heat exchanger with inlet and outlet water ports.

The energy balance on the adsorbent bed control volume for adsorber/desorber can be described as:

$$C_{HE}\frac{dT_b}{dt} = m_{ads,HE}\frac{dw_b}{dt}\Delta h_{ad} - \left(\frac{\dot{m}_{v,i}}{N_{HE}}\right)Cp_v(T_b - T_{evap}) + \dot{Q}_{heat/cool} \quad (9)$$

where, C_{HE} is the thermal capacity of the adsorbent bed heat exchanger (adsorbent + adsorbate + metal). Eq. (9) is valid for the bed in adsorption mode as well in desorption mode. However, in desorption mode the term $\dot{m}_{v,i}\, Cp_v\,(T_b - T_{evap})$ in Eq. (9) must not be included since the desorbed vapor is assumed to be at the same temperature as that of the bed. The term on the left-hand side of Eq. (9) represents the amount of sensible heat required to heat or cool the bed (including; adsorbent, the adsorbate as well as the metallic parts in the bed) during adsorption or desorption processes. The first tem on the right-hand side refers to the heat due to either the adsorption or desorption process. The second term shows the sensible heat of the adsorbed water vapor, which is the sensible heat required to heat up the vapor from the evaporation temperature up to the bed temperature during adsorption. Finally, the third term represents the total amount of heat ($\dot{Q}_{heat/cool}$) released to the cooling water or provided by the heating water depending on the operation mode of the bed.

An alternative expression to the standard effectiveness-NTU formulation has been developed here in order to determine the heat exchanged between the system components and the heat transfer fluid (secondary water) under non-steady conditions. The effect of inlet and outlet temperature differences on the heat flux are taken into account. The heat transfer $\dot{Q}_{heat/cool}$ is represented by the following correlation

$$\dot{Q}_{heat/cool} = \varepsilon_{HE}\dot{m}_{w,HE}Cp_w\left[\alpha(T_{wi,HE} - T_b) + (1-\alpha)\left(\frac{T_{wo,HE} - T_b}{1 - \varepsilon_{HE}}\right)\right] \quad (10)$$

where the parameter α corresponds to the weighting factor of the temperature difference between the inlet and outlet water temperatures and the temperature of the bed. This parameter was adjusted by comparing the numerical predictions with the experimental results. A value of $\alpha = 0.8$ (i.e. 80%) of the inlet temperature difference and 20% of the outlet temperature difference was found to produce good results for a wide range of operating conditions. The effectiveness of the adsorbent bed heat exchanger (ε_{HE}) is given by:

$$\varepsilon_{HE} = 1 - \exp\left(-\frac{UA_{total,HE}}{\dot{m}_{w,HE}Cp_w}\right) \quad (11)$$

The thermal losses to the inert masses due to the alternate bed heating and cooling have been taken into consideration in the model. The heat transfer from the inlet secondary water to the inlet header and port tube $\dot{Q}_{losses,i}$ is evaluated with an expression similar to Eq. (10) by:

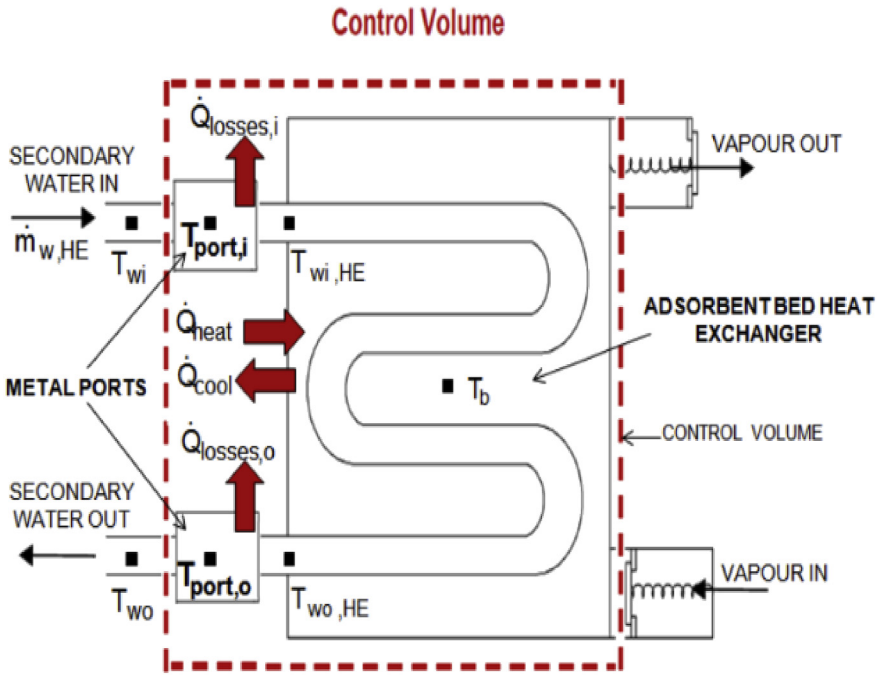

Fig. 4. Single adsorbent bed heat exchanger with the considered control volume (red dashed line). (For interpretation of the references to colour in this figure legend, the reader is referred to the web version of this article.)

$$\dot{Q}_{losses,i} = \varepsilon_{port,i}\dot{m}_{w,HE}Cp_w\left[\alpha(T_{wi} - T_{port,i}) + (1-\alpha)\frac{T_{wi,HE} - T_{port,i}}{1-\varepsilon_{port,i}}\right] \quad (12)$$

The heat transfer from the outlet secondary water to the outlet header and port tube $\dot{Q}_{losses,o}$ is given by:

$$\dot{Q}_{losses,o} = \varepsilon_{port,o}\dot{m}_{w,HE}Cp_w\left[\alpha(T_{wo,HE} - T_{port,o}) + (1-\alpha)\frac{T_{wo} - T_{port,o}}{1-\varepsilon_{port,o}}\right] \quad (13)$$

where, $\varepsilon_{port,i}$ and $\varepsilon_{port,o}$ are the effectiveness of inlet and outlet header and ports respectively. The temperature of the inlet header $T_{port,i}$ and outlet header $T_{port,o}$ is given by their corresponding energy conservation equations as:

$$C_{port,i} = \frac{dT_{port,i}}{dt} = \dot{Q}_{losses,i} \quad (14)$$

$$C_{port,o} = \frac{dT_{port,o}}{dt} = \dot{Q}_{losses,o} \quad (15)$$

where, $C_{port,i}$ and $C_{port,o}$ are the thermal capacity of the inlet and outlet metal ports of the bed, respectively. As a matter of fact, they are simply evaluated by dividing the total mass of the heat exchanger including the inlet and outlet headers, multiplied by the metal specific heat. In this may it is possible to accurately take into account the total energy employed for the alternate heating and cooling of the total metal mass of the bed.

The temperatures of the secondary water at the inlet of the adsorbent bed heat exchanger $T_{wi,HE}$ and at the outlet of the heat exchanger $T_{wo,HE}$ are given by:

$$C_{wport,i}\frac{dT_{wi,HE}}{dt} = \dot{m}_{w,HE}Cp_w(T_{wi} - T_{wi,HE}) - \dot{Q}_{losses,i} \quad (16)$$

$$C_{wHE}\frac{dT_{wo,HE}}{dt} = \dot{m}_{w,HE}Cp_w(T_{wi,HE} - T_{wo,HE}) - \dot{Q}_{losses,o} \quad (17)$$

where, $C_{wport,i}$ is the thermal capacity of the secondary water inside the inlet header and $C_{w,HE}$ is the thermal capacity of the secondary water inside the adsorbent heat exchanger.

Finally, the temperature of the secondary water (T_{wo}) leaving the bed (from the outlet header) is given by the following equation:

$$C_{wport,o}\frac{dT_{wo}}{dt} = \dot{m}_{w,HE}Cp_w(T_{wo,HE} - T_{wo}) - \dot{Q}_{losses,o} \quad (18)$$

where, $C_{wport,o}$ is the thermal capacity of the secondary water inside the outlet header.

The continuity equation at the adsorbent bed provides the necessary link between the vapor mass in the bed ($m_{v,b}$) the uptake variation (w_b) and the vapor flow rates leaving ($m_{v,out}$) or entering ($m_{v,in}$) the bed:

$$\frac{dm_{v,b}}{dt} = -m_{ads,b}\frac{dw_b}{dt} + \dot{m}_{v,i} - \dot{m}_{v,o} \quad (19)$$

Equilibrium is not assumed in the bed. Therefore, it is necessary to introduce an equation for the pressure. The differential equation for the pressure (P_b) in the adsorbent bed assuming that non-condensable gasses had been totally removed can be expressed in the following way when a perfect gas behavior is assumed.

$$\frac{dP_b}{dt} = P_b\left(\frac{1}{T_b}\frac{dT_b}{dt} + \frac{1}{m_{v,b}}\frac{dm_{v,b}}{dt}\right) \quad (20)$$

In order to calculate the vapor flow through the interconnecting pipes and valves and between the sorption beds, the condenser, and the evaporator. In practice, vapor velocities must be kept low in order to minimize pressure losses, hence the vapor flow can be considered non-compressible. Therefore, the instantaneous flow rates, $\dot{m}_{v,in}$ and $\dot{m}_{v,out}$, can be calculated as follows:

$$\dot{m}_{v,in} = \begin{cases} 0 & \text{If } P_b < P_{evap} \ (a) \\ A_{evap}\sqrt{2\rho_v(T_{evap}, P_{evap})(P_{evap} - P_b)} & \text{If } P_b \le P_{evap} \ (b) \end{cases} \quad (21)$$

$$\dot{m}_{v,out} = \begin{cases} 0 & \text{If } P_b < P_{cond} \ (a) \\ A_{cond}\sqrt{2\rho_v(T_b, P_b)(P_b - P_{cond})} & \text{If } P_b \ge P_{cond} \ (b) \end{cases} \quad (22)$$

where, a set of convenient reed valves has been considered to connect the bed with evaporator and condenser. The valves are considered to close instantaneously when the flow is reversed and having a constant effective area A_{evap} and A_{cond} when the valves are open. A dynamically varying model for the valves could be easily incorporated if a slow motion were detected in experiments.

The above set of Eqs. (9–20) constitutes a system of ODEs for w_b, T_b, $T_{port,i}$, $T_{port,o}$, $T_{wi,HE}$, $T_{wo,HE}$, T_{wgi}, T_{wo}, P_b and $m_{v,b}$ for each bed. Furthermore, it is possible to calculate the refrigerant flow between the sorption beds and the evaporator/condenser according to the operation mode of the bed.

3.3.2. Condenser model

During the desorption process, the condenser is connected to the bed where the refrigerant (desorbed vapor) can be condensed and delivered to the evaporator through an expansion valve. Since the refrigerant comes from the desorber bed as vapor at higher temperature $T_{cond,i}$ and at the same pressure as in the condenser P_{cond}, the energy balance equation for the vapor region surrounding the condenser tubes can be given as follows:

$$\dot{Q}_c = \dot{m}_{cond}\left[Cp_v(T_{cond,i} - T_{cond}) + \Delta h_{fg}(T_{cond})\right] \quad (23)$$

The left-hand side of equation Eq. (23) represents the total amount of heat transferred to the cooling water. The first term on the right-hand side shows the sensible heat of the vapor being cooled from the temperature of the refrigerant leaving the bed (desorbed vapor) down to the temperature of condensation. The second term represents the total amount of latent heat involved in the change of state from saturated vapor to saturated liquid.

The rate of heat released ($\dot{Q}_c$) from the refrigerant to the secondary water can again be evaluated by:

$$\dot{Q}_c = -\varepsilon_{cond}\dot{m}_{w,sec}Cp_w\left[\alpha(T_{sec,i} - T_{cond}) + (1-\alpha)\frac{T_{sec,o} - T_{cond}}{1-\varepsilon_{cond}}\right] \quad (24)$$

The temperature of the secondary water ($T_{sec,o}$) at the outlet of the condenser can be estimated by the following equation:

$$C_{cond}\frac{dT_{sec,o}}{dT} = \dot{m}_{w,sec}Cp_w(T_{sec,i} - T_{sec,o}) + \dot{Q}_c \quad (25)$$

The term on the left-hand side of equation Eq. (25) refers to the energy variation of the metallic tubes and cooling water in the condenser. The first term on the right-hand side represents enthalpy change of the water flow across the condenser. The second term shows the amount of heat transferred from the cooling water flow to the condenser.

The mass balance equation for the vapor, which links the variation of vapor mass in the condenser with the incoming mass flow from the bed ($\dot{m}_{v,o}$) and the condensation rate ($\dot{m}_{cond}$) can be written as

$$\frac{dm_{v,cond}}{dt} = \dot{m}_{cond,i} - \dot{m}_{cond} \tag{26}$$

where, $\dot{m}_{con,i}$ is the refrigerant flow entering the condenser which corresponds to the total flow of water vapor desorbed from the bed ($\dot{m}_{con,i} = \dot{m}_{v,o}$).

The mass balance equation for the liquid in the condenser can be written as:

$$\frac{dm_{l,cond}}{dt} = \dot{m}_{cond} - \dot{m}_{cond,o} \tag{27}$$

where, $\dot{m}_{l,con}$ is the mass of liquid water in the condenser and $\dot{m}_{con,o}$ is the refrigerant (liquid water) flow from the condenser to the evaporator.

Hence, the volume of liquid water in the condenser ($V_{l,cond}$) can be estimated as:

$$\frac{dV_{l,cond}}{dt} = \frac{1}{\rho_w}\frac{dm_{1,cond}}{dt} \rightarrow \frac{dV_{l,cond}}{dt} = \frac{\dot{m}_{cond} - \dot{m}_{cond,o}}{\rho_w} \tag{28}$$

The link between the liquid volume ($V_{l,cond}$) and the volume occupied by the vapor in the condenser ($V_{v,cond}$) can be expressed by:

$$\frac{dV_{v,cond}}{dt} = -\frac{dV_{l,cond}}{dt} \tag{29}$$

The equation of state for the vapor provides a way to evaluate the variation of the pressure as a function of the variation of the vapor mass, volume, and temperature:

$$P_{cond} = \frac{RT_{cond}}{V_{v,cond}}\frac{m_{v,cond}}{M_w} \rightarrow \frac{d}{dt}(P_{cond}, V_{v,cond}) = \frac{d}{M_w}\frac{d}{dt}(T_{cond}, m_{v,cond}) \tag{30}$$

where, M_w is the water molar mass [kgmol^{-1}]; R is the universal gas constant [mbarm^3 kg^{-1} K^{-1}]; $m_{v,cond}$ is the water vapor mass in the condenser [kg]; is the volume of water vapor in the condenser [m^3]; T_{cond} is the temperature in the condenser [K]; P_{cond} is the pressure in condenser [mbar].

Since the refrigerant inside the condenser is in a saturated state, the following equation provides a way to relate the temperature variation with the pressure in the condenser:

$$T_{cond} = T_{sat}(P_{cond}) \rightarrow \frac{dT_{cond}}{dt} = \frac{dT_{sat}(P_{cond})}{dP_{cond}}\frac{dP_{cond}}{dt} \tag{31}$$

By the product rule and replacing Eq. (31), the following differential equation for the pressure in the condenser is obtained:

$$\frac{dP_{cond}}{dt} = \frac{\frac{P_{cond}}{m_{v,cond}}\left(\frac{dm_{v,cond}}{dt}\right) - \frac{P_{cond}\left(\frac{dV_{v,cond}}{dt}\right)}{V_{v,cond}}}{1 - \frac{P_{cond}}{T_{cond}}\left(\frac{dT_{sat}}{dP_{cond}}\right)} \tag{32}$$

By solving the set of differential Eqs. (25–32) in time, the following unknowns are found for each bed: P_{cond}, $m_{v,cond}$, $V_{v,cond}$ and $T_{sec,o}$. Furthermore, it is possible to calculate the condensation rate, the volume of the liquid in the condenser and the temperature in the condenser according to the saturation hypothesis.

3.3.3. Evaporator model

Since the refrigerant enters the evaporator as liquid at higher pressure and temperature ($P_{cond,o}$, $T_{cond,o}$), the energy balance equation for the refrigerant in the evaporator can be given by:

$$\dot{Q}_E = \dot{m}_{evap}\left[\Delta h_{fg}(T_{evap}) - Cp_w(T_{cond,o} - T_{evap})\right] \tag{33}$$

where, $\dot{m}_{evap}$ is the evaporation rate, T_{evap} is the evaporator temperature, Δ_{hfg} is the specific heat of vaporization T_{evap}. The first term on the right-hand side of Eq. (33) represents the total amount of latent heat involved in the change of state from saturated liquid to saturated vapor. The second term represents the sensible heat required to cool the incoming water condensed from the condensation temperature to the evaporation temperature.

The rate of heat provided by the secondary water (i.e. chilled water) to the refrigerant ($\dot{Q}_E$) can be expressed by:

$$\dot{Q}_E = \varepsilon_{evap}\dot{m}_{w,chill}Cp_w\left[\alpha(T_{chill,i} - T_{evap}) + (1-\alpha)\frac{T_{chill,o} - T_{evap}}{1 - \varepsilon_{evap}}\right] \tag{34}$$

where, ε_{evap} is the evaporator effectiveness; $\dot{m}_{w,chill}$ is the chilled water mass flow [Kgs^{-1}]; Cp_w is the specific heat capacity of the water [Jkg^{-1} K^{-1}]; $T_{chill,i}$ and $T_{chill,o}$ are the inlet and outlet temperatures of the evaporator secondary water (i.e. chilled water).

The temperature of the chilled water at the outlet of the evaporator ($T_{chill,o}$) can be estimated by:

$$C_{evap}\frac{dT_{chill,o}}{dt} = \dot{m}_{w,chill}Cp_w(T_{chill,i} - T_{chill,o}) - \dot{Q}_E \tag{35}$$

The term on the left-hand side of Eq. (35) refers to the temporal variation of the internal energy contained in the metal tubes and the water mass in the evaporator. The first term on the right-hand side shows the amount of sensible heat provided by the secondary water. Finally, the second term refers to the total amount of heat exchanged with the refrigerant.

The mass balance equation for the vapor, which links the variation of vapor mass in the evaporator with the out coming mass flow from the evaporator ($\dot{m}_{eva,o}$) and the evaporation rate ($\dot{m}_{evap}$) can be written as:

$$\frac{dm_{v,evap}}{dt} = \dot{m}_{evap} - \dot{m}_{evap,o} \tag{36}$$

where, $\dot{m}_{evap}$ is the evaporation rate, and $\dot{m}_{evap,o}$ is the refrigerant flow leaving the evaporator which corresponds to the total flow of vapor adsorbed by the bed ($\dot{m}_{evap,o} = \dot{m}_{v,i}$).

The pressure in the evaporator is based on the vapor state equation which provides a way to evaluate the variation of the pressure as a function of the vapor mass ($m_{v,evap}$), vapor volume

($V_{v,evap}$) and temperature (T_{evap}) can be described by:

$$P_{evap} = \frac{RT_{evap}}{V_{v,evap}} \frac{m_{v,evap}}{M_w} \rightarrow \frac{d}{dt}(P_{evap}, V_{v,evap}) = \frac{d}{M_w} \frac{d}{dt}(T_{evap}, m_{v,evap}) \quad (37)$$

Since the refrigerant (water vapor) inside the evaporator is in a saturated state. The following equation provides a way to relate the variation of the temperature with the pressure in the evaporator:

$$T_{evap} = T_{sat}(P_{evap}) \rightarrow \frac{dT_{evap}}{dt} = \frac{dT_{sat}(P_{evap})}{dP_{evap}} \frac{dP_{evap}}{dt} \quad (38)$$

The differential equation for the pressure in the evaporator can be obtained by:

$$\frac{dP_{evap}}{dt} = \frac{\frac{P_{evap}}{m_{v,evap}}\left(\frac{dm_{v,evap}}{dt}\right)}{1 - \frac{P_{evap}}{T_{evap}}\left(\frac{dT_{sat}}{dP_{evap}}\right)} \quad (39)$$

By solving the set of differential equation for each system component of Eqs. (35–39) in time, the following unknowns are found for each bed: P_{evap}, $m_{v,evap}$, $V_{v,evap}$, $T_{chill,o}$. Furthermore, it is possible to calculate the evaporation rate, the volume of the liquid in the evaporator and the temperature in the evaporator accordingly with the saturation hypothesis.

4. Measurement of system performance

The model is capable of calculating the amount of heat exchanged in each component and consequently, the performance of the system. The cooling capacity $\dot{Q}_{chill}$ is given by the following equation:

$$\dot{Q}_{chill} = \dot{m}_{w,chill} Cp_w \int_0^{t_{cycle}} (T_{chill,i} - T_{chill,o}) dt \quad (40)$$

The condenser capacity $\dot{Q}_{cond}$ is given by:

$$\dot{Q}_{cond} = -\dot{m}_{w,sec} Cp_w \int_0^{t_{cycle}} (T_{sec,i} - T_{sec,o}) dt \quad (41)$$

The heating capacity of the bed $\dot{Q}_{heat}$ is given by the following equation:

$$\dot{Q}_{heat} = \dot{m}_{hw,b} Cp_w \int_0^{t_{cycle}} (T_{hw,i} - T_{hw,o}) dt \quad (42)$$

The cooling capacity of the bed $\dot{Q}_{cool}$ is given by the following equation:

$$\dot{Q}_{cool} = -\dot{m}_{cw,b} Cp_w \int_0^{t_{cycle}} (T_{cw,i} - T_{cw,o}) dt \quad (43)$$

The performance of the adsorption system is mainly characterized by the cooling capacity of the system (Q_{chill}) and the coefficient of performance (COP). The COP is the ratio between the heat extracted by the evaporator and the heat source input to the bed as the following:

$$COP = \frac{\dot{Q}_{chill}}{\dot{Q}_{heat}} = \frac{\int_0^{t_{cycle}} (\dot{m}Cp)_{chill}(T_{chill,in} - T_{chill,o}) dt}{\int_0^{t_{cycle}} (\dot{m}Cp)_{des}(T_{hw,in} - T_{hw,o}) dt} \quad (44)$$

where, t_{cycle} denotes the total cycle time. Experimentally, the cooling capacity and the COP was obtained from the measurements of heat transfer fluid temperatures and mass flow rates at a fixed cycle time of 360 s, which is the optimum for the characteristics of the considered system.

The system of first-order ordinary differential equations (ODEs) described above was implemented in MATLAB® as an S-Function and solved dynamically in Simulink® by the solver ode23tb (stiff/TR-BDF2). The solver uses Runge-Kutta technique to solve the system of ODEs and it gives accurate solutions with high speed of convergence. Fig. 5 shows a simplified structure of the system model with a set of inputs, state variables, and outputs.

Furthermore, the model requires several parameters which are kept constant throughout the simulation. These parameters are related to the (i) thermos-physical properties of the water, adsorbent, and other components of the system and (ii) physical design of the system. The main parameters used in the model are listed in Table 3.

5. Simulation results and model validation

As mentioned before, the experimental tests were performed in two operation modes (configurations); without heat recovery and with heat recovery. These modes are explained in the next sections.

5.1. First operation mode: tests performed without heat recovery

Fig. 6 shows a comparison between the simulated and experimental results for the pressure and outlet water temperature profiles of the adsorbent beds at the operating conditions shown in Table 4. As it can be observed, the numerical model predicts well the pressures and outlet water temperatures of adsorbent beds determined from the experimental data with ± 5% error for both the pressures and outlet water temperatures. The predicted pressures, however, show some relatively small deviations of at the switching region. The main difference being that the experimental pressure reacts faster than the modeled one. This can be due, either to the corresponding temperature and pressure sensor delays, or to the fact that the kinetics of the adsorption/desorption processes are not perfectly taken into account in the model. Generally, the model predicted fairly well the whole dynamics of the system.

Fig. 7 shows the simulated and experimental results of the temperature and pressure profiles corresponding to the condenser and evaporator. As it can be seen, again, the simulation results show a good agreement with the experimental results regardless the hypothesis assumed in the model and capturing most of the observed dynamics. A small delay between the experimental pressure and the calculated one can be also seen.

In regard to the system performance, Fig. 8 shows a comparison between the calculated and measured values of the instantaneous evaporator and condenser capacities. It can be observed that there is a good agreement between experimental and simulated results taking into account the approximate nature of the model and the noise on the performance evaluated from the experimental results. The average cooling capacity at permanent conditions has a value of 2.1 kW. The average condenser capacity was about 2.215 kW.

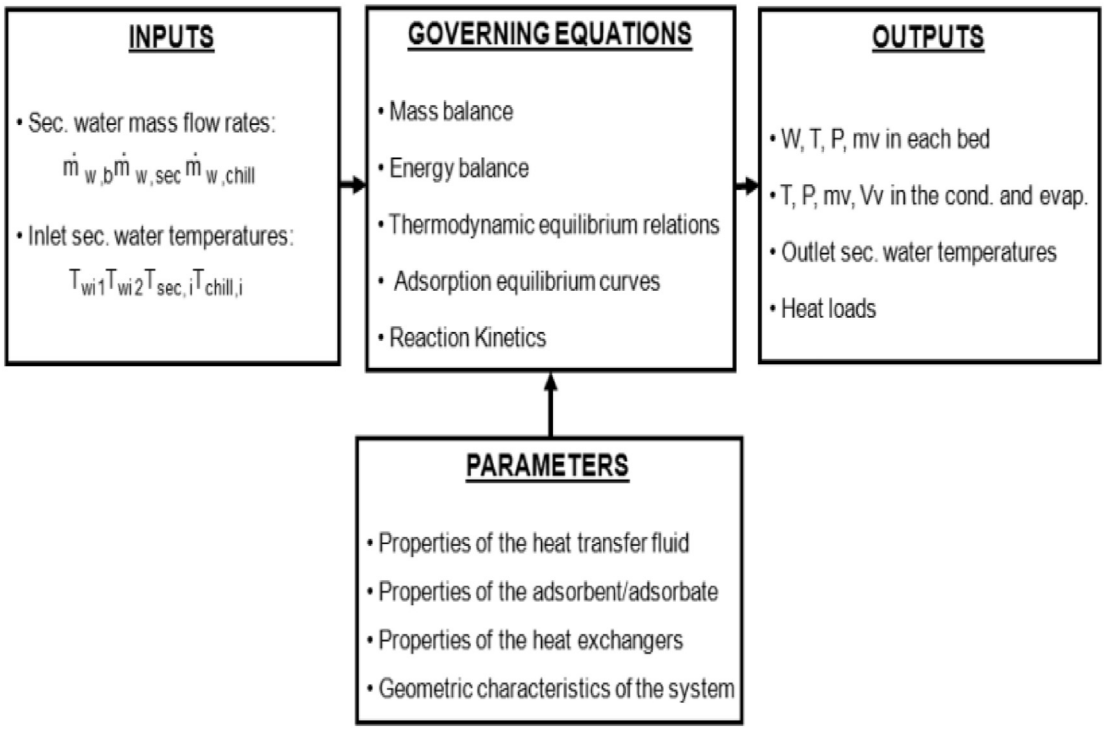

Fig. 5. Simplified structure of the adsorption system model.

Fig. 9 shows the equilibrium and non-equilibrium uptake evaluated by the model. During the first half cycle time, the adsorbent in the bed is in desorption and the water content of the adsorbent is decreased to about 0.034 kg/kg. In the second half cycle, the adsorbent in the bed is in adsorption and the water content of the adsorbent increases to about 0.088 kg/kg. The beds exchange their roles in the next half cycle and return to the first mode in the third cycle. As it can be seen, the adsorption phase is found to be a bit slower than the desorption one, with a more or less constant difference between the actual uptake and the one which would correspond to equilibrium. Along the desorption period, the difference between equilibrium and actual uptake is higher at the beginning but rapidly decreases with time. The difference between the potentially possible uptake difference and the one which is actually obtained, shows the important role of the sorption kinetics on the performance of the system. The agreement between both the instantaneous measured and calculated results and the prediction of the global performance indirectly validates the employed modeling of the sorption kinetics.

Finally, Fig. 10 shows the Dühring diagram calculated from the bed pressure and temperature for both measured and calculated data. The equilibrium uptake is estimated from the instantaneous recordings of bed pressure and temperature experimentally. While the model appears to predict the behavior of the Dühring diagram with reasonable accuracy, the prediction shows some deviations from the experiments, particularly during the adsorption period. The main reason for this deviation is the temperature of the bed. However it is difficult to know if the prediction of this temperature

Table 3
Values of parameters adopted in the simulation.

Symbol	Value	Units	Observations
cp_w	4182	J Kg^{-1} K^{-1}	[54]
ρ_w	1014	J Kg^{-1} K^{-1}	[54]
h_w	2248	Wm^{-2} K^{-1}	[54]
$C_{pads,o}$	750	J Kg^{-1} K^{-1}	[52]
Cp_{met}	890	J Kg^{-1} K^{-1}	[55]
k_{met}	160	Wm^{-2} K^{-1}	[55]
k_1	0.019	s^{-1}	[53]
k_2	906	K	[53]
$m_{w,HE}$	0.3276	kg	ECN system prototype
$m_{w,porti}$	0.0938	kg	Assumed to be 1/3 of $m_{w,HE}$
$m_{w,porto}$	0.0938	kg	Assumed to be 1/3 of $m_{w,HE}$
$m_{met,HE}$	1.012	kg	ECN system prototype
$m_{port,i}$	0.1518	kg	Assumed to be 1/6 of $m_{met,HE}$
$m_{port,o}$	0.1518	kg	Assumed to be 1/6 of $m_{met,HE}$
$m_{ads,HE}$	1	kg	ECN system prototype
N_{HE}	3	–	ECN system prototype
V_b	0.0108	m^3	ECN system prototype
V_{cond}	0.0231	m^3	ECN system prototype
V_{evap}	0.0128	m^3	ECN system prototype

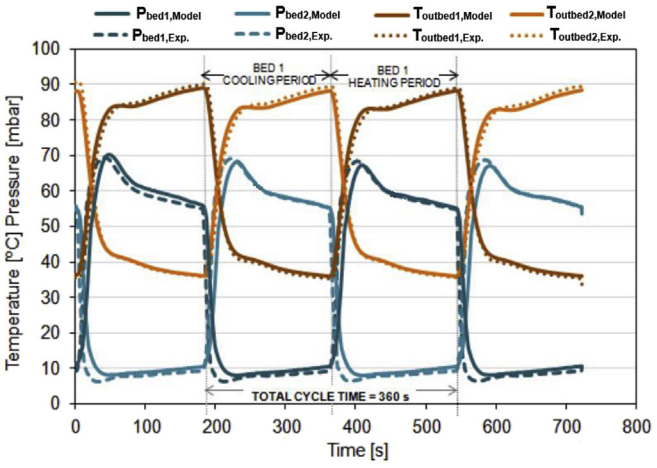

Fig. 6. Experimental and model prediction of pressure and outlet temperature of adsorbent beds.

Table 4
The nominal operating condition for the two-bed adsorption chiller.

Hot water inlet		Cooling water inlet (cond. + adsorber)		Chilled water inlet	
Temp. [°C]	Flow rate [kgs^{-1}]	Temp. [°C]	Flow rate [kgs^{-1}]	Temp. [°C]	Flow rate [kgs^{-1}]
90	0.20	33	0.20	15	0.13

is good or not since one must take into account that there is a high uncertainty in the evaluation of the bed temperature, given that the experimental value corresponds only to the readings of a single temperature sensor inserted into the bed, so the measurements are local. This is the reason why the comparison is shown in Fig. 6 includes the outlet water temperature from the bed instead of the sorbent temperature. The inertia of the temperature measurement together with temperature variation across the sorbent could explain the differences in the model results and the experimental ones. In general, the agreement in the total variation of uptake is good. According to the simulation results, the minimum temperature reached by the bed at the end of the adsorption phase was 36 °C, with a maximum uptake of about 10 wt%, while the maximum temperature reached by the bed at the end of the regeneration phase was 88 °C, with a minimum uptake of about 3 wt%.

The overall good agreement between calculated and experimental results, proves that the developed model is an adequate tool to assist the design and optimization of adsorption cooling systems.

5.2. Second operation mode: tests performed with heat recovery operation

Fig. 11(a–d) shows a comparison between the simulated and experimental results at the above-mentioned operating conditions for the first 800 s for different parameters.

Comparing these results with those obtained previously for the first operation mode (without heat recovery), it can be observed that there are almost no differences in the behavior of the system with the cycle time. The major differences in the system when operating in heat recovery mode are due to the amount of heat that is saved when heating the secondary water, and not due to the operation of the beds. The experimental and simulation results showed a considerable increase in the COP when the heat recovery is performed. Notice that the time delay when switching between

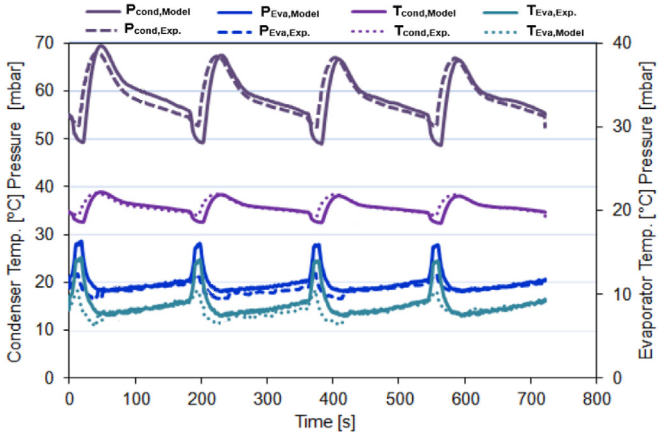

Fig. 7. Comparison between experimental and numerical results of temperature and pressure at condenser and evaporator.

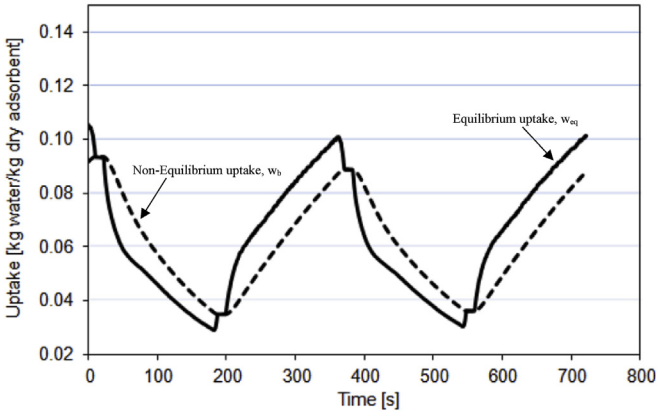

Fig. 9. Equilibrium and non-equilibrium uptake evolution for one bed (desorber).

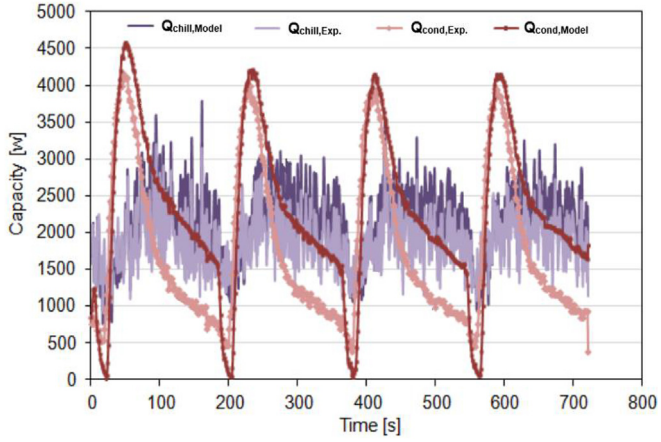

Fig. 8. Comparison between calculated and experimental results for evaporator cooling capacity and condenser capacity.

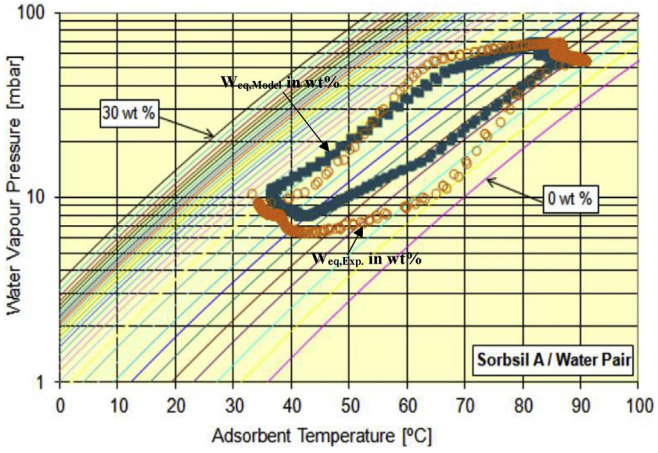

Fig. 10. Calculated and measured Dühring diagram of the Silica gel (Sorbsil A)/water adsorption system at rated conditions.

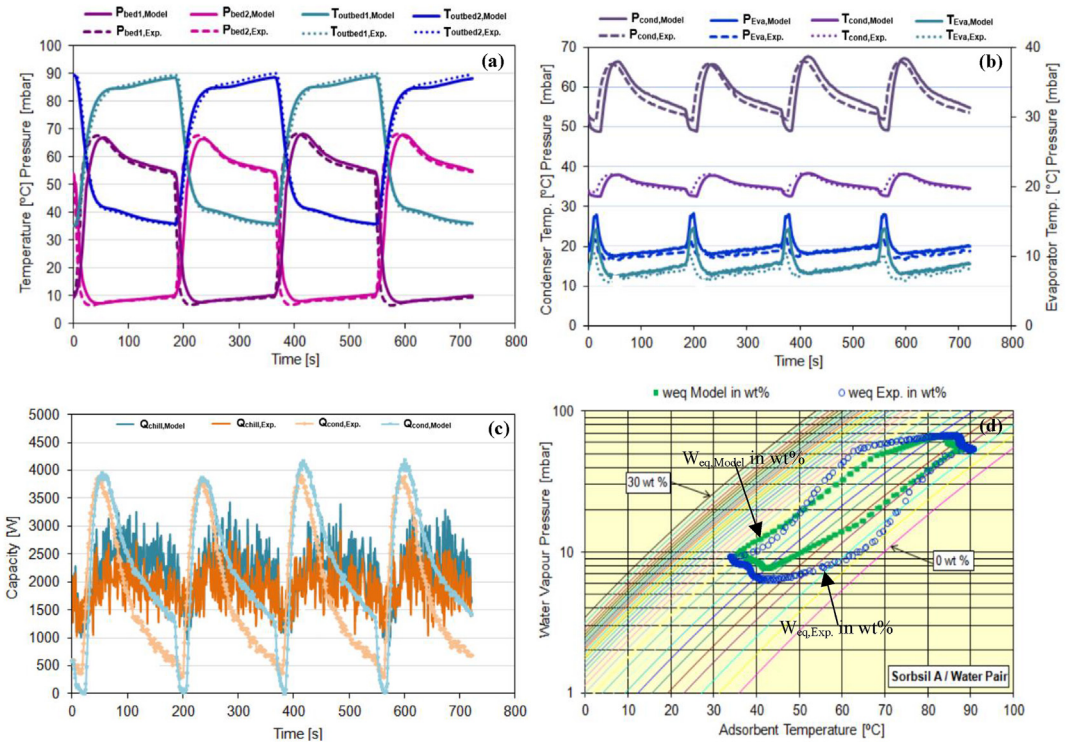

Fig. 11. Comparison between calculated and measured results - 2nd Operation Mode (heat recovery mode): **(a)** Pressure and outlet temperature profiles of adsorbent beds, **(b)** Temperature profiles and pressures at condenser and evaporator, **(c)** Cooling capacity and condenser capacity, **(d)** Dühring diagram of the Silica gel/water adsorption system at rated conditions.

Table 5
System performance at different operation modes.

Operation mode	Experimental results		Simulation results		Error (%)	
	$\dot{Q}_{chill,Exp.}$ [kW]	COP	$\dot{Q}_{chill,Model}$ [kW]	COP	$\dot{Q}_{chill,Model}$	COP
1st mode: No heat recovery	1.9	0.31	2.1	0.35	10.5	12.9
2nd mode: Heat recovery	2	0.45	2.2	0.50	10.0	11.1

inlet and outlet valves of the beds' secondary water circuits is very small (around 20 s).

Again, a good agreement between the simulation and the experimental results with heat recovery operation can be observed, and this further confirms the validity of the proposed model.

6. System performance evaluation

Table 5 summarizes the performance of the proposed system under different operation modes and at the same nominal operating conditions. As it can be seen, clearly, the system with heat recovery provides considerably greater values of COP and a slight positive effect on the evaporator cooling capacity. Both experimental and simulation results show a very similar increase in the coefficient of performance (COP) when the heat recovery is performed and a similar effect on the cooling capacity was found. This proves again the suitability of the model as a tool to assist the design and optimization of cooling sorption systems.

Based on the simulation results, the system is able to produce about 2.1 kW of average cooling capacity with COP of 0.35. If the auxiliary heat recovery circuit is considered, the system is able to produce about 2.2 kW of cooling capacity with COP of 0.50. Based on experimental results, the system is able to produce a mean cooling capacity of about 1.9 kW with COP of 0.31 for the second configuration mode, and a mean cooling capacity of 2.0 kW with COP of 0.45 for the second configuration mode. The typical experimental error when determined the cooling capacity was about 5%. The uncertainty on the COP is consequently higher (10%).

It can be concluded that the heat recovery operation has a strong positive effect on the system performance (COP), and a slight positive effect on the cooling capacity. This operation strategy can be considered as one of the key points to improve the performance of adsorption systems. However, with heat recovery operation, the system becomes more complex (more piping, valves, and more complicated management).

7. Conclusions

In this first part, Part I of a two-part study, a theoretical and experimental investigation were performed on a silica gel/water adsorption chiller driven by engine waste heat. An improved non-equilibrium dynamic model is developed. The model takes into account the mass transfer resistance, the pressure and temperature of each system component as well as the vapor flow in between these components. The simulation results were validated against instantaneous experimental measurements realized at ECN laboratory of an adsorption chiller prototype. The experimental tests were conducted using two different system configurations with

and without auxiliary heat recovery modes.

The results showed that the system is able to produce an average cooling capacity of 2.1 kW (producing chilled water at 13 °C) with COP of 0.35 at the rated conditions. Both experimental and simulation results showed a considerable increase in the system COP (by about 43%) when the heat recovery operation is performed. A considerable good agreement between simulation and experimental results for both instantaneous and averaged data at different operation modes were obtained. The developed model has proven to be an adequate tool to assist the design and optimize the operation of adsorption cooling systems. In Part II, the validated model is used to simulate and optimize the performance of an on-board adsorption system (implemented in a car) under different real start-up and ambient conditions to get a comfortable temperature in the automobile cabin.

Acknowledgements

This work has been partially supported by the Thermally Operated Mobile Air Conditioning Systems (TOPMACS). The authors are very grateful to the Energy Research Center of Netherlands (ECN) for their support in the experimental work.

References

[1] Edwin Raj R, Joseph S, Daniel B. Development of energy saving and environment friendly aluminum hybrid composite materials for vehicle applications. Adv Mater Res 2013;768:195–8.
[2] Ahmed S, Ahmed A, Harby K, Mahmoud S. A state of the art of hybrid adsorption desalination-cooling systems. Energy Sustain Dev 2016;58:692–703.
[3] Harby K, Gebaly D, Koura N, Hassan M. Performance improvement of vapor compression cooling systems using evaporative condenser: an overview. Renew Sustain Energy Rev 2016;58:347–60.
[4] Verde M, Harby K, de Boer Robert, Corberán JM. Performance evaluation of a waste-heat driven adsorption system for automotive air-conditioning: Part II-Performance optimization under different real driving conditions. Energy 2016;115:996–1009.
[5] Hamdy M, Askalny A, Harby K, Kora N. An overview on adsorption cooling systems powered by waste heat from internal combustion engine. Renew Sustain Energy Rev 2015;51:1223–34.
[6] Azhar B, Ang L, Kyaw T, Kim C, Wongee C. Pressurized adsorption cooling cycles driven by solar/waste heat. Appl Therm Eng 2014;67:106–13.
[7] Farrington R, Rugh J. Impact of vehicle air-conditioning on fuel economy, tailpipe emissions, and electric vehicle range. In: Proceeding of the earth technologies forum, Washington, D.C; 2000.
[8] Wang D, Li H, Li D, Xia Y, Zhang J. A review on adsorption refrigeration technology and adsorption deterioration in physical adsorption systems. Renew Sustain Energy Rev 2010;14:334–53.
[9] Wai S, Loh A, Bin I, Kim C, Won G. Experimental investigation of a small-scale thermally driven pressurized adsorption chiller. Heat Trans Res 2015;46:311–32.
[10] Kyaw T, Young-Deuk K, Aung M, Won G, Kim C. Entropy generation analysis of an adsorption cooling cycle. Int J Heat Mass Transf 2013;60:143–55.
[11] Aung M, Ng K, Kyaw T, Young-Deuk K. Experimental investigation on the optimal performance of Zeolite-water adsorption chiller. Appl Energy 2013;102:582–90.
[12] Verde M, Harby K, Corberán JM. Optimization of thermal design and geometrical parameters of a flat tube-fin adsorbent bed for automobile air-conditioning. Appl Therm Eng 2017;111:489–502.
[13] Mohamed G, Harby K, Ahmed A, Bidyut B. Adsorption isotherms and kinetics of activated carbon/difluoroethane adsorption pair: theory and experiments. Int J Refrig 2016;7:196–205.
[14] Wang D, Xia Z, Wu J. Design and performance prediction of a novel zeolite-water adsorption air conditioner. Energy Convers Manag 2006;47:590–610.
[15] Zhang L. Design and testing of an automobile waste heat adsorption cooling system. Appl Therm Eng 2000;20:103–14.
[16] Ramji H, Leo S, Abdullah M. Parametric study and simulation of a heat driven adsorber for air conditioning system employing activated carbon-methanol working pair. Appl Energy 2014;113:324–33.
[17] Zhong Y, Fang T, Wert KL. An adsorption air conditioning system to integrate with the recent development of emission control for heavy-duty vehicles. Energy 2011;36:4125–35.
[18] Verde M, Cortés L, Corberán JM, Sapienza A, Vasta S, Restuccia G. Modelling of an adsorption system driven by engine waste heat for truck cabin A/C. Performance estimation for a standard driving cycle. Appl Therm Eng 2010;30:1511–22.
[19] Zhang LZ, Wang L. Performance estimation of an adsorption cooling system for automobile waste heat recovery. Appl Therm Eng 1997;17:1127–39.
[20] Maggio G, Freni A, Restuccia G. A dynamic model of heat and mass transfer in a double-bed adsorption machine with internal heat recovery. Int J Refrig 2006;29:589–600.
[21] Sami S, Tribes C. An improved model for predicting the dynamic behaviour of adsorption systems. Appl Therm Eng 1996;16:149–61.
[22] Schicktanz M, Núñez T. Modelling of an adsorption chiller for dynamic system simulation. Int J Refrig 2009;32:588–95.
[23] Miyazaki T, Akisawa A. The influence of heat exchanger parameters on the optimum cycle time of adsorption chillers. Appl Therm Eng 2009;29:2708–17.
[24] Voyiatzis E, Pavlos A, Markatos N. Heat-exchanger design and switching-frequency effects on the performance of a continuous type solar adsorption chiller. Appl Energy 2008;85:1237–50.
[25] Restuccia G, Freni A, Maggio G. A zeolite-coated bed for air conditioning adsorption systems: parametric study of heat and mass transfer by dynamic simulation. Appl Therm Eng 2002;22:619–30.
[26] Miltkau T, Dawoud B. Dynamic modeling of the combined heat and mass transfer during the adsorption/desorption of water vapor into/from a zeolite layer of an adsorption heat pump. Int J Therm Sci 2002;41:753–62.
[27] Melkon T, Birgul T, Ayse E. A novel approach to enhance heat and mass transfer in adsorption heat pumps using the zeolite-water pair. Microporous Mesoporous Mater 1999;27:1–10.
[28] Zheng W, Worek W. Effect of operating conditions on the performance of two-bed closed-cycle solid-sorption heat pump systems. J Sol Energy Eng 1995;117:181–6.
[29] Liu Y, Leong K. The effect of operating conditions on the performance of zeolite/water adsorption cooling systems. Appl Therm Eng 2005;25:1403–18.
[30] Marletta L, Maggio G, Freni A, Ingrasciotta M, Restuccia G. A non-uniform temperature non-uniform pressure dynamic model of heat and mass transfer in compact adsorbent beds. Int J Heat Mass Transf 2002;45:3321–30.
[31] Alam K, Saha B, Kang Y, Akisawa A, Kashiwagi T. Heat design effect on the performance of silica gel adsorption refrigeration systems. Int J Heat Mass Transf 2000;43:4419–31.
[32] Niazmand H, Dabzadeh I. Numerical simulation of heat and mass transfer in adsorbent beds with annular fins. Int J Refrig 2012;35:581–93.
[33] Chua H, Ng C, Wang Yap C, Wang X. Transient modeling of a two-bed silica gel-water adsorption chiller. Int J Heat Mass Transf 2004;47:659–69.
[34] Zhang Z. A three dimensional non-equilibrium model for an intermittent adsorption cooling system. Sol Energy 2000;69:27–35.
[35] Jiangzhou S, Wang R, Lu Y, Xu Y, Wu J. Experimental study on locomotive driver cabin adsorption air conditioning prototype machine. Energy Convers Manag 2005;46:1655–65.
[36] Jiangzhou S, Wang R, Lu Y, Xu YX, Wu JY, Li ZH. Locomotive driver cabin adsorption air-conditioner. Renew Energ 2003;28:1659–70.
[37] Jiangzhou S, Wang RZ, Lu YZ, Xu YX, Wu JY. Experimental investigations on adsorption air-conditioner used in internal-combustion locomotive driver-cabin. Appl Therm Eng 2002;22:1153–62.
[38] Wu W, Zhang H, Men C. Performance of a modified zeolite 13X-water adsorptive cooling module powered by exhaust waste heat. Int J Therm Sci 2011;50:2042–9.
[39] Lu YZ, Wang RZ, Jianzhou S, Xu YX, Wu JY. Practical experiments on an adsorption air conditioner powered by exhausted heat from a diesel locomotive. Appl Therm Eng 2004;24:1051–9.
[40] Suzuki, M. Application of adsorption cooling systems to automobiles, Heat Recovery Syst CHP 199313;4;335–340.
[41] Tamainot-Telto Z, Metcalf SJ, Critoph RE. Novel compact sorption generators for car air conditioning. Int J Refrig 2009;32:727–33.
[42] Grisel RH, Smeding SF, Boer RD. Waste heat driven silica gel/water adsorption cooling in trigeneration. Appl Therm Eng 2010;30:1039–46.
[43] Vasta S, Freni A, Sapienza A, Costa F, Restuccia G. Development and lab-test of a mobile adsorption air-conditioner. Int J Refrig 2012;35:701–8.
[44] Ali Syed, Anutosh C. Thermodynamic modelling and performance study of an engine waste heat driven adsorption cooling for automotive air-conditioning. Appl Therm Eng 2015;90:54–63.
[45] Demir H, Mobedi M, Ülkü S. A review on adsorption heat pump: problems and solutions. Renew Sust Energ Rev 2008;12:2381–403.
[46] Lambert M, Jones J. Review of regenerative adsorption heat pumps. J Thermophys Heat Transf 2005;19:471–85.
[47] Chekirou W, Boussehain R, Feidt M, Karaali A, Boukheit N. Numerical results on operating parameters influence for a heat recovery machine. Energy Proced 2011;6:202–16.
[48] Douss N, Meunier E, Sun M. Predictive model and experimental results for a two-adsorber solid adsorption heat pump. Ind Eng Chem Res 1988;27:310–6.
[49] European project TOPMACS-Thermally Operated Mobile Air-Conditioning Systems, funded by the European Comission under the 6th European Community framework program (Contract Ref. TST4-CT-2005–012471). Retrieved from: http://ec.europa.eu/research/transport/projects/items/topmacs_en.htm.
[50] Ineos Group Limited, Technical information on adsorbent materials (Sorbsil A). Retrieved from: http://www.ineos.com/.
[51] Cacciola G, Restuccia G. Reversible adsorption heat pump: a thermodynamic model. Int J Refrig 1995;18:100–6.

[52] Restuccia G, Aristov Y, Maggio G, Cacciola G, Tokarev M. Performance of sorption systems using selective water sorbents. In: Proc. of the international sorption heat pump conference-ISHPC99, Munich, Germany; 1999. p. 219–23.
[53] Wang D, Xia Z, Wu J. Design and performance of a novel zeolite-water adsorption air conditioner. Energ Convers Manag 2006;47:590–610.
[54] Mills A. Heat transfer. second ed. Upper Saddle River: Prentice Hall; 1999.
[55] Alam KC, Kang Y, Saha BB, Akisawa A, Kashiwagi T. A novel approach to determine optimum switching frequency of a conventional adsorption chiller. Energy 2003;28:1021–37.

Nomenclature

A: area, m^2
COP: coefficient of performance
C_p: specific heat, Jkg^{-1} k^{-1}
m: mass, kg
$M_{ads,b}$: total mass of dry adsorbent packed in each bed, kg
$\dot{m}$: mass flow rate, kg s^{-1}
P: pressure, mbar
R: universal gas constant, mbar m^3 kg^{-1} K^{-1}
T: temperature, k
T_{wi}: water temperature at the inlet of the bed, K
$T_{wi,HE}$: water temperature at the inlet of the heat exchanger, K
T_{wo}: water temperature at the outlet of the bed, K
$T_{wo,HE}$: water temperature at the outlet of the heat exchanger, K
$UA_{tot,HE}$: overall thermal conductance of the adsorbent heat exchanger, W K^{-1}
V: volume, m^3
w: uptake, kg kg^{-1}

Subscripts

b: bed
chill: chilled water
cond: condenser
des: desorption
eq: equilibrium
evap: evaporator
HE: heat exchanger
i: inlet
l: liquid
out: outlet
Port,i: inlet port
Port,o: outlet port
sec: secondary
tot: total
W: water
w: uptake, kg kg^{-1}

Greek Letters

ρ: Density, kg m^{-3}
ε: effectiveness
Δh_{ad}: enthalpy of adsorption, J kg^{-1}
τ_{cycle}: full cycle time [s]

ECN
Westerduinweg 3
1755 LE Petten
The Netherlands

P.O. Box 1
1755 LG Petten
The Netherlands

T +31 88 515 4949
F +31 88 515 8338
info@ ecn.nl
www.ecn.nl